Calculation of the average velocity vector with DUDI

Anastasiia Ershova

January 11, 2025

1 Algorithm

The DUDI algorithm evaluates the number density n of dust particles with radii R within the range $R_{min} < R < R_{max}$ at a specified point defined by radial distance r from the moon's center, polar angle α, and eastern longitude β. This is achieved by integrating the phase-space number density $n(r, \alpha, \beta, v, \theta, \lambda, R_{min} < R < R_{max})$ over all possible velocity vectors of the dust particles at the given point, where (v θ, λ) are the spherical components of the velocity vector (see Ershova and Schmidt, 2021, for mathematical derivation and a detailed description of the algorithm).

In DUDI, the dust particle velocity is expressed in a local horizontal coordinate system, defined as follows: the x-axis points toward the local north, the z-axis points toward the zenith, and the y-axis completes the right-handed coordinate system. The azimuth λ is measured clockwise from the x-axis. During the integration over velocity v, the velocity vector components in the local horizontal coordinate system (v, θ, λ) are computed at every integration step. This allows for the transformation of the velocity vector from spherical coordinates to Cartesian coordinates as follows:

$$v_x = v \sin\theta \cos\lambda, \quad v_y = -v \sin\theta \sin\lambda, \quad v_z = v \cos\theta.$$

Subsequently, these Cartesian coordinates are transformed via coordinate system rotation from the local horizontal coordinate system to the moon-centered coordinate system to obtain the vector $\mathbf{v} = (v_x, v_y, v_z)$. Knowing velocity allows for the computation of the dust flux as

$$\mathbf{F}(r,\ \alpha,\ \beta, R_{min} < R < R_{max}) = \sum_{i=1}^{N} n(r, \alpha, \beta, v_i, \theta_i, \lambda_i, R_{min} < R < R_{max}) \mathbf{v}_i \mathrm{d}v_i,$$

where N is the order of the numerical quadrature formula used for integration.

The velocities of particles on outbound trajectories and those on inbound trajectories partially cancel each other when summed. Therefore, it is beneficial to compute the fluxes for the upward and downward directions separately, providing a clearer representation of the dust dynamics at (r, α, β). The total number density at the point of interest can also be divided into outbound and inbound parts:

$$n(r, \alpha, \beta, R_{min} < R < R_{max}) = n_{up} + n_{down},$$

where

$$n_{up} = \sum_{\theta_i < \pi/2} n(r, \alpha, \beta, v_i, \theta_i, \lambda_i, R_{min} < R < R_{max}) \mathrm{d}v_i,$$

and

$$n_{down} = \sum_{\theta_i \geq \pi/2} n(r, \alpha, \beta, v_i, \theta_i, \lambda_i, R_{min} < R < R_{max}) \mathrm{d}v_i.$$

Then, the mean velocity vector can be computed separately for the upward and downward moving particles as

$$\mathbf{v}_{up} = \frac{1}{n_{up}(r, \alpha, \beta, R_{min} < R < R_{max})} \sum_{\theta_i < \pi/2} n(r, \alpha, \beta, v_i, \theta_i, \lambda_i, R_{min} < R < R_{max}) \mathbf{v}_i \mathrm{d}v_i,$$

$$\mathbf{v}_{down} = \frac{1}{n_{down}(r, \alpha, \beta, R_{min} < R < R_{max})} \sum_{\theta_i \geq \pi/2} n(r, \alpha, \beta, v_i, \theta_i, \lambda_i, R_{min} < R < R_{max}) \mathbf{v}_i \mathrm{d}v_i.$$

The algorithm described above is implemented in the DUDI package version 1.2.0 as a separate subroutine, `DUDI_mean_velocity`. It receives the same input as the subroutine `DUDI` and outputs an array of 8 elements:

- $\mathbf{v}_{up}$: the averaged upward velocity vector (3 real numbers),
- $\mathbf{v}_{down}$: the averaged downward velocity vector (3 real numbers),
- n_{up}: the number density of particles on outbound trajectories (1 real number),
- n_{down}: the number density of particles on inbound trajectories (1 real number).

The vectors $\mathbf{v}_{up}$ and $\mathbf{v}_{down}$ are expressed in the same moon-centered coordinate system as the input parameters (r, α, β), with the velocity vector components provided in Cartesian coordinates. If fluxes are the quantities of interest, they can be computed as

$$\mathbf{F}_{up} = n_{up}\mathbf{v}_{up}, \quad \mathbf{F}_{down} = n_{down}\mathbf{v}_{down}$$

2 Results

Let us examine the results of the subroutine `DUDI_mean_velocity`. We consider an example case with a single dust source located on a moon with the mass and mean radius of Enceladus. The source ejects dust particles with speeds uniformly distributed between 0 and 230 m/s, and the zenith angle of the ejection velocity is uniformly distributed between 0° and 90°. The ejection velocity is independent of particle size; hence, we do not consider the particle size distribution. Figures 1a and 1b illustrate the field of average velocity vectors in a plane containing the source and the moon's center.

The maximum ejection velocity is slightly below the escape velocity of this moon (239 m/s). As a result, all ejected material falls back, and no particles follow hyperbolic trajectories. However, the maximum velocity averaged among particles moving upward ($\theta < 90°$) is higher than the mean velocity of particles falling back. The highest mean velocities of upward moving grains are observed on the opposite side from the source. In these distant regions, particles on inbound trajectories are significantly more abundant. While trajectories on which dust grains continue to gain altitude at nearly 180° angular distance from the source are improbable, they are not entirely impossible but would require higher velocities. Figure 1a has several points near the moon's surface where no upward-moving particles are present. Thus, although the mean velocity of upward

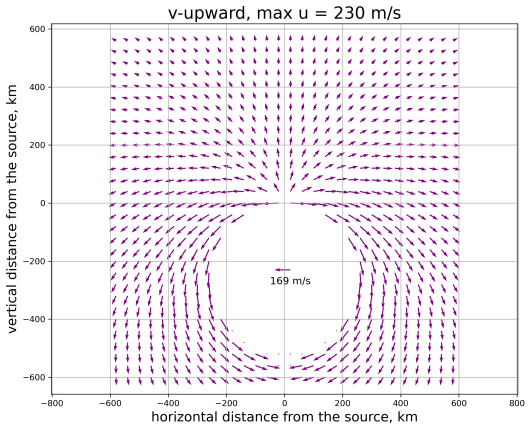

(a) Averaging only among the particles on outbound trajectories.

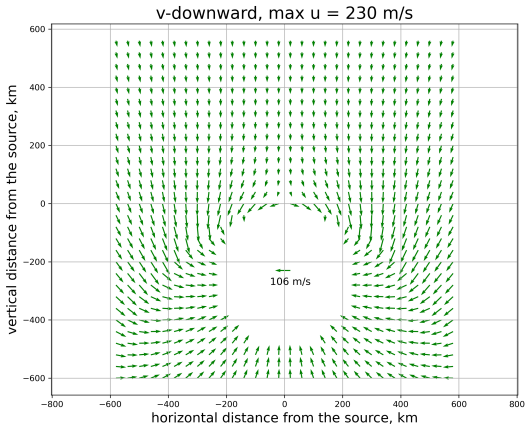

(b) Averaging only among the particles on inbound trajectories.

Figure 1: Vector field of the average velocity vector in the plane. The arrow inside the moon is plotted for scale, with its length corresponding to the maximum average velocity obtained for the points shown.

moving dust grains is higher at some points than the one of the grains falling back, the momentum is conserved via likelihood of such velocities.

Figures 2 and 3 show the distribution of the magnitudes and zenith angles of the mean velocities as functions of the distance from the moon's center r (expressed in moon radii, r_M) and the angular distance from the dust source $\Delta\phi$. The test sample points range from $r = r_M$ to $r = 3.5r_M$ in radial distance from the moon's center and from 4° to 171° in angular distance from the dust source.

The points with zero average velocity in Fig. 2a result from the absence of particles on outbound trajectories at these locations. Specifically, there are no particles on outbound trajectories at zero altitude above the moon's surface and at locations 30 or 60 km above the surface with large $\Delta\phi$. These points are excluded from the zenith angle plot (Fig. 3a) because the zenith angle of a zero-vector is undefined. The range of the obtained mean velocities is (60, 168) m/s for upward-moving particles and (30, 108) m/s for particles

falling back.

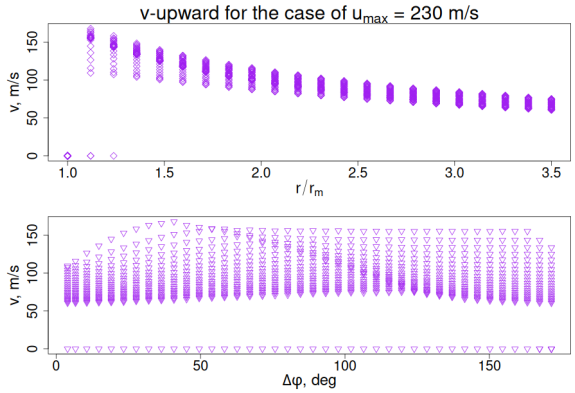

(a) Averaging only among the particles on outbound trajectories.

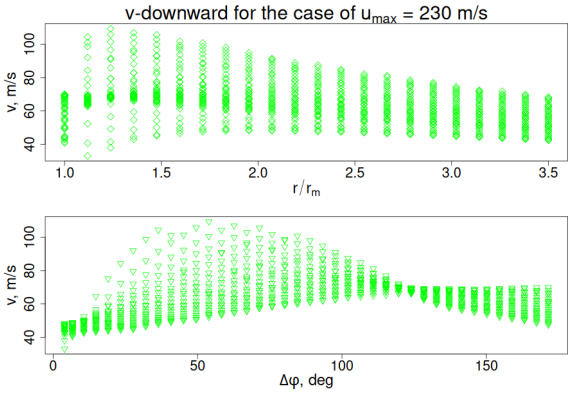

(b) Averaging only among the particles on inbound trajectories.

Figure 2: Distribution of average speed v at different altitudes and angular distances from the source.

Both upward and downward mean velocities exhibit a decreasing trend with increasing altitude. Near the source, there is also a depletion of particles having high velocities. The particles falling back with high velocities must be ejected at high velocities and are therefore more likely to fall back at significant distances from the source. On the other hand, the particles ejected with small velocities can still be moving upward at small $\Delta\phi$ bringing down the mean upward-velocity in this region too.

The range of average velocities obtained for different $\Delta\phi$ narrows with increasing altitude; this trend is more pronounced for upward-moving particles. The variation in mean velocity values with $\Delta\phi$ is much more pronounced for downward-moving dust grains. At approximately 120° from the source, the range of average velocities computed for points at various altitudes reaches its minimum and increases for larger $\Delta\phi$.

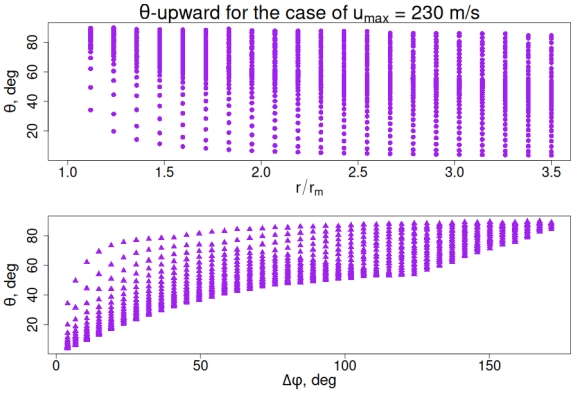

(a) Averaging only among the particles on outbound trajectories.

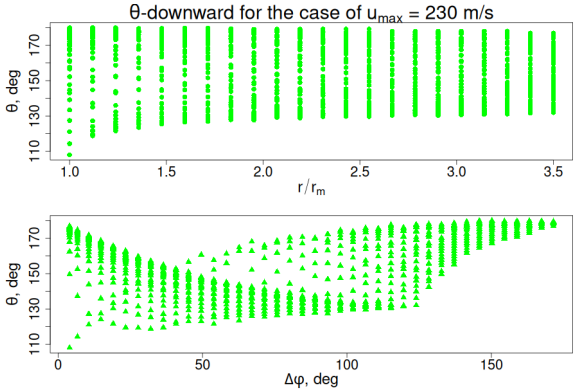

(b) Averaging only among the particles on inbound trajectories.

Figure 3: Distribution of average angle θ at different altitudes and angular distances from the source.

The range of possible mean zenith angles θ shows little variation with radial distance, except for the smallest sampled r. The mean θ of particles moving upward increases with

$\Delta\phi$, as the particles approach the apocenter of their trajectories. In contrast, particles moving downward exhibit steeper trajectories at large $\Delta\phi$. At very small $\Delta\phi$, particles also tend to move steeply upward or downward, as this region contains particles that were ejected nearly vertically.

Figures 4 and 5 show the distributions of average velocities v and zenith angles θ for a source on the same moon ejecting dust with speeds uniformly distributed between 0 and 600 m/s. In this case, more than half of the particles are set on hyperbolic trajectories. The distributions of the downward-moving particles remain almost the same, as particles ejected faster than the escape velocity do not contribute to this population.

Comparing Figs. 4a and 5a with Figs. 2a and 3a, we observe the contribution of particles on unbound trajectories. Specifically, the range of mean v has expanded toward higher values, while the lower nonzero limit remains nearly unchanged. Additionally, the distribution of points within the ranges obtained for fixed r or $\Delta\phi$ has changed, showing a double-peaked structure for each fixed r and a strong dominance of particles on hyperbolic trajectories at $\Delta\phi <\sim 70°$. Across all r and $\Delta\phi$, steeper trajectories are more probable compared to the case where ejection velocities are only below the escape velocity.

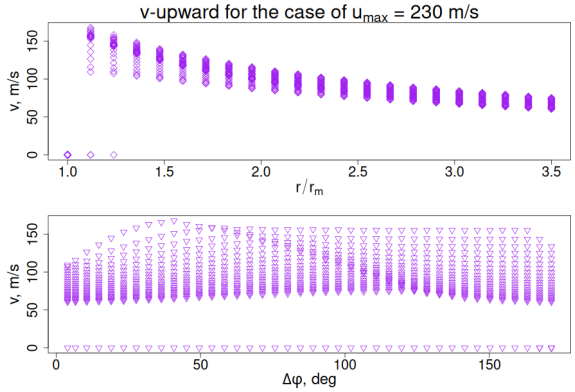

(a) Averaging only among the particles on outbound trajectories.

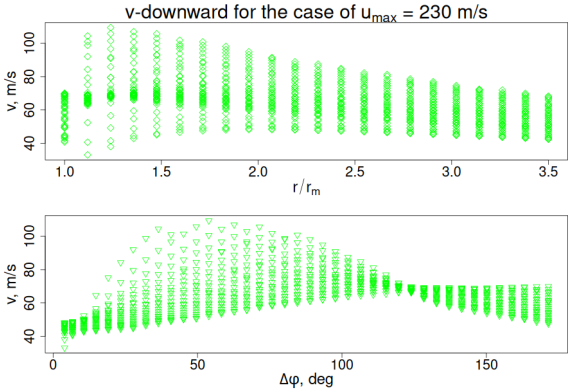

(b) Averaging only among the particles on inbound trajectories.

Figure 4: Distribution of average speed v at different altitudes and angular distances from the source.

References

Ershova, A. and Schmidt, J. (2021). Two-body model for the spatial distribution of dust ejected from an atmosphereless body. *Astronomy & Astrophysics*, 650:A186.

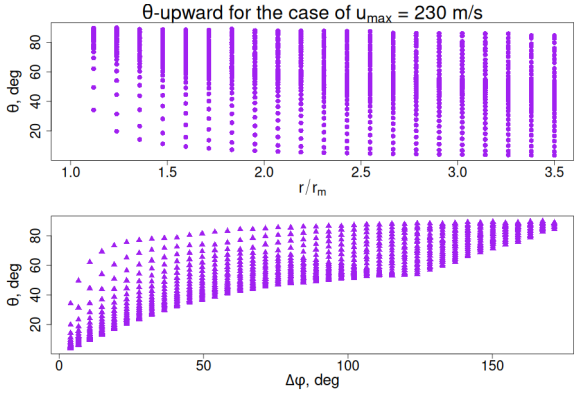

(a) Averaging only among the particles on outbound trajectories.

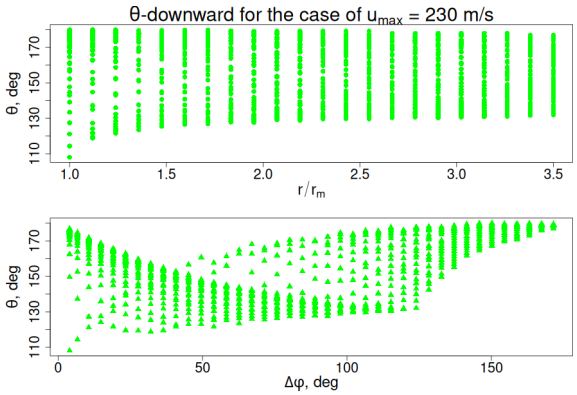

(b) Averaging only among the particles on inbound trajectories.

Figure 5: Distribution of average angle θ at different altitudes and angular distances from the source.